increased recombination failure for the smallest chromosomes and to a corresponding increase in aneuploid embryos in SCP3-null females.

What then is the role of SCP3 and how does its absence cause chromosomal nondisjunction? SCP3 expression is restricted to meiotic prophase I cells, disappearing during diakinesis in female oocytes (*14*). The structural changes seen in meiotic chromatin due to SCP3 absence strongly suggest that nondisjunction is caused by errors that initially occur at pachytene. It was also found that the SCP1 fiber in *SCP3*-deficient pachytene oocytes contained axial gaps, indicating incomplete homolog synapsis. Incorrect homolog alignment could affect the crossing-over process that generates chiasmata. SCP1 homologs in yeast (Zip1) and *Drosophila* [C(3)G] have been shown to be important for both synapsis and crossing-over, and their absence results in a high level of nondisjunction (*15, 16*). Mutations in these two proteins that introduce noncontiguous axial gaps in their respective TF structures reduce the levels of meiotic exchange and crossover interference. In addition, mutations in genes that affect crossover interference randomize crossover distribution between chromosomes, such that chromosomes may fail to cross over and therefore nondisjoin (*2, 17, 18*). The observed changes in chromatin structure and SCP1 organization along the homologs in SCP3-null oocytes could therefore affect crossover interference, affecting both chiasma positioning and frequency.

The increased embryo death in older $SCP3^{-/-}$ females is notable. A reduced oocyte pool in humans has been proposed to result in a premature increase in aneuploidy and embryo death (*19*). By this model, a shortened reproductive life span, resulting from a substantial loss of oocytes in the developing $SCP3^{-/-}$ ovary could explain the increased embryo death. Alternatively, SCP3 absence could have two effects on chromosomal nondisjunction, an early effect seen as a reduction in chiasmata number and a later effect that only manifests itself in older females. The second model could be explained as a two-hit mechanism, as previously suggested for aging human oocytes (*20*). The first hit would be due to a reduction in crossover interference resulting in suboptimal positioning of chiasmata along the chromosomes, whereas the second hit would occur due to an inability of older oocytes to resolve chiasmata located at certain chromosomal regions. The model system described here should thus be valuable toward understanding the basis for meiotic nondisjunction and age-dependent aneuploidy in human oocytes.

References and Notes

1. T. Hassold, P. Hunt, *Nature Rev. Genet.* **2**, 280 (2001).
2. D. Zickler, N. Kleckner, *Annu. Rev. Genet.* **33**, 603 (1999).
3. K. Schmekel, B. Daneholt, *Trends Biochem. Sci.* **5**, 239 (1995).
4. K. Nasmyth, *Annu. Rev. Genet.* **35**, 673 (2001).
5. J. A. C. Schalk *et al.*, *Chromosoma* **107**, 540 (1998).
6. L. Yuan *et al.*, *J. Cell Biol.* **142**, 331 (1998).
7. J. Pelttari *et al.*, *Mol. Cell. Biol.* **21**, 5667 (2001).
8. L. Yuan *et al.*, *Mol. Cell* **5**, 73 (2000).
9. M. R. Hoja, J. G. Liu, L. Yuan, E. Brundell, C. Höög, data not shown.
10. N. M. Lawrie, C. Tease, M. A. Hulten, *Chromosoma* **140**, 308 (1995).
11. M. Tarsounas, T. Morita, R. E. Pearlman, P. B. Moens, *J. Cell Biol.* **147**, 207 (1999).
12. L. K. Anderson, A. Reeves, L. M. Webb, T. Ashley, *Genetics* **151**, 1569 (1999).
13. Supplementary figure and details of experimental procedures are available on *Science* Online at www.sciencemag.org/cgi/content/full/296/5570/1115/DC1
14. C. A. Hodges, R. LeMaire-Adkins, P. A. Hunt, *J. Cell Sci.* **114**, 2417 (2001).
15. K. S. Tung, G. S. Roeder, *Genetics* **149**, 817 (1998).
16. S. L. Page, R. S. Hawley, *Genes Dev.* **15**, 3130 (2001).
17. M. Sym, G. S. Roeder, *Cell* **79**, 283 (1994).
18. D. P. Kaback, D. Barber, J. Mahon, J. Lamb, J. You, *Genetics* **152**, 1475 (1999).
19. J. Kline, A. Kinney, B. Levin, D. Warburton, *Am. J. Hum. Genet.* **67**, 395 (2000).
20. N. E. Lamb *et al.*, *Nature Genet.* **14**, 400 (1996).

21. Supported by the Swedish Cancer Society, The Swedish Research Council, Pharmacia Corporation, Petrus and Augusta Hedlunds Stiftelse, and Karolinska Institutet. We thank E. Brundell and M.-L. SpÅngberg for technical assistance, C. Heyting for antisera, and P. A. Hunt, J. Schimenti, K. Schmekel, M. Sjöberg, and B. Daneholt for helpful discussions.

6 February 2002; accepted 29 March 2002

Ablation of Insulin-Producing Neurons in Flies: Growth and Diabetic Phenotypes

Eric J. Rulifson,[1,3]* Seung K. Kim,[1,2] Roel Nusse[1,3]

In the fruit fly *Drosophila*, four insulin genes are coexpressed in small clusters of cells [insulin-producing cells (IPCs)] in the brain. Here, we show that ablation of these IPCs causes developmental delay, growth retardation, and elevated carbohydrate levels in larval hemolymph. All of the defects were reversed by ectopic expression of a *Drosophila* insulin transgene. On the basis of these functional data and the observation that IPCs release insulin into the circulatory system, we conclude that brain IPCs are the main systemic supply of insulin during larval growth. We propose that IPCs and pancreatic islet β cells are functionally analogous and may have evolved from a common ancestral insulin-producing neuron. Interestingly, the phenotype of flies lacking IPCs includes certain features of diabetes mellitus.

The *Drosophila* genome contains five *Drosophila* insulinlike peptide genes (*dilp1* through *-5*) with significant homology to mouse and human insulins and two others with far less similarity (*dilp6* and *-7*). These genes are expressed in tissues ranging from early embryonic mesoderm to small clusters of larval brain neurons, ventral nerve cord neurons, salivary gland, and midgut (*1*). Using messenger RNA (mRNA) in situ hybridization, we established that the most prominent insulin gene expression during larval stages, a period of intensive feeding and rapid growth, is within two bilaterally symmetric clusters of neurosecretory cells in the pars intercerebralis region of the protocerebrum (fig. S1).

An 859–base pair promoter fragment, comprised of sequences immediately 5′ of *dilp2*, was sufficient to drive gene expression in the small clusters of larval brain neurons that express *dilp1*, *-2*, *-3*, and *-5* (fig. S1). To assess the role of the brain IPCs as an insulin-producing endocrine system, we ablated the brain IPCs using the *dilp2* promoter to express the cell death–promoting factor, Reaper (*2*). The IPC ablation results in deficiency of brain neuron-derived insulin only (fig. S2). IPC ablation caused undergrowth phenotypes, developmental delays, and lethality similar to *Drosophila* insulin receptor (DInR) mutants (*1*, *3*). To rule out an underlying cause of these phenotypes other than insulin deficiency, such as non-IPC death from Reaper or loss of other essential brain IPC functions, we used a heat shock–inducible *dilp2* transgene with ubiquitous expression to reverse the effect of the IPC ablation.

We quantified the defect in growth by comparing larval length after 120 hours of development, a time at which synchronized cultures of normal larvae will reach wandering third instar and puparium formation. [Larval phenotypes are shown in (fig. S3).] After IPC ablation, larvae attained a mean length only 58% of normal size (Fig. 1A, center). Larvae with IPCs ablated but expressing the inducible *dilp2* transgene had

[1]Department of Developmental Biology, [2]Department of Medicine (Oncology Division), [3]Howard Hughes Medical Institute, Beckman Center B300, Stanford University, Stanford, CA 94305–5329, USA.

*To whom correspondence should be addressed. E-mail: rulifson@cmgm.stanford.edu

their mean length rescued to 88% of normal (Fig. 1A, right). The developmental time to reach wandering third instar and puparium formation was approximately 5 days in normal larvae but lengthened to 12 days in larvae after IPC ablation, a developmental rate similar to that observed in animals homozygous for loss-of-function mutations in DInR (*1*). Larvae with ablated IPCs that expressed the inducible *dilp2* transgene required approximately 6 days to reach puparium formation. Thus, systemic DILP2 expression was sufficient to compensate for IPC ablation. That brain IPC ablation is rescued by *dilp2* alone suggests insulin made by brain IPCs may be partially redundant.

IPC ablation produced small-sized adults of normal proportion (fig. S3). Examination of adult wings revealed reductions in both cell size and number after IPC ablation. [Wing phenotypes are shown in (fig. S3).] Under the strongest condition of IPC ablation, mean wing size was reduced to 61% of normal, whereas wing cell number and size were reduced to 72% and 85% of normal, respectively (Fig. 1B). Under a less severe regimen of IPC ablation, mean wing size was reduced to 74% of normal, with reductions in cell number and size to 81% and 91% of normal, respectively (Fig. 1B). As in larval growth, the *dilp2* transgene effectively reversed the effects of IPC ablation on wing growth and, in fact, caused a slight overgrowth effect (Fig. 1B), possibly due to the 20% lengthening of developmental time that allowed more growth. The overall reduction in cell size and number after IPC ablation is similar to that in DInR (*1*) and IRS1-4 mutants (*4*). This, together with our observation that brain IPC-derived insulins can activate the DInR in vitro (fig. S4), suggests that brain IPCs are a key source of insulin for this growth control pathway.

We also investigated the role of brain IPCs and insulin in the regulation of carbohydrate metabolism. Trehalose is a disaccharide composed of two glucose molecules and is the principal blood sugar in many insects (*5*). Using the same heat shock regimen, we compared the combined concentration of glucose and trehalose in the hemolymph of wandering third instar larvae, a brief and discrete developmental stage before puparium formation when feeding has

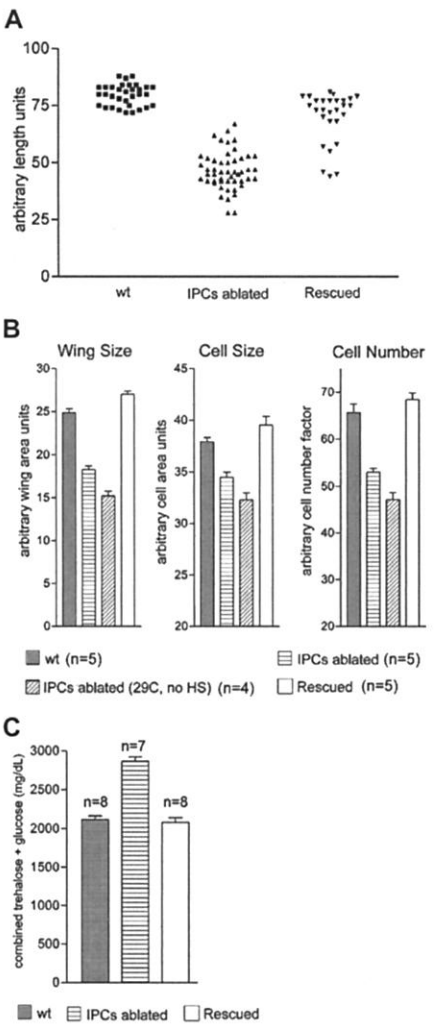

Fig. 1. Ablation of brain IPCs leads to decreased animal size, which affects both cell size and number, and elevated hemolymph carbohydrate concentration. These effects are rescued by *dilp2* transgene activity. (**A**) Scatter plot showing relative size values for individual larvae of wild-type (left), IPC-ablated *dilp2* promoter>*UAS-rpr* (center), and "rescued" *dilp2* promoter>*UAS-rpr* with the *hs-dilp2* transgene (right) after 120 hours of development under heat shock regimen. (**B**) Mean and SEM (error bars) values of relative wing size, cell size (measured by area), and cell number for wings from adults of same genotype and conditions as in (A). Diagonally hatched column gives values for IPC-ablated *dilp2* promoter>*UAS-rpr* females grown at a constant 29°C. (**C**) Total combined trehalose and glucose concentration (mg/dl) in hemolymph of wandering third instar larvae of genotypes and treatment as in (A). Wild type (mean = 2074, SEM = 27.78), IPC-ablated (mean = 2867, SEM = 55.08), and rescued (mean = 2081, SEM = 61.10). Each sample value is taken from pooled hemolymph of three larvae.

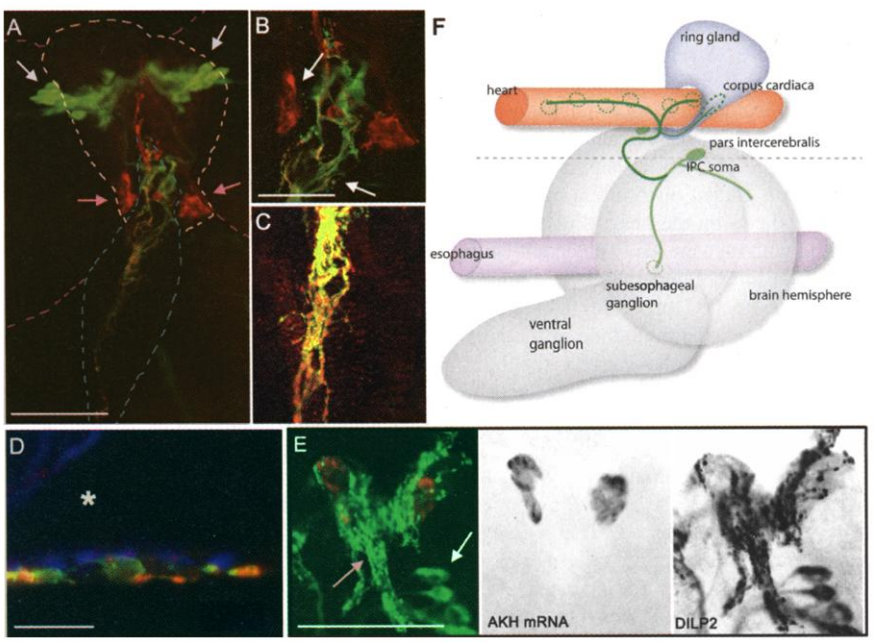

Fig. 2. Anatomy of brain IPCs. (**A**) Brain hemispheres (outlined in pink dashed line), ring gland (outlined in white dashed line), and heart (outlined in blue dashed line) of a wandering third instar larva (dorsal side facing out of page), labeled with *dilp2* promoter>*UAS-mGFP* (green) and immunostained with antibody to DILP2 (red). Scale bar, 100 μm. Clusters of IPC cell bodies within the brain hemispheres (white arrows) extend processes out of the brain to the heart and to the corpora cardiaca (pink arrows). (**B**) Close-up image of (A) shows IPC processes (green) entering the corpora cardiaca (arrows). DILP2 peptide (red) is localized in the IPC processes (yellow in merge) and in the corpora cardiaca cells outside the IPC processes. Scale bar, 50 μm. (**C**) Close-up image of (A) shows IPC processes terminating along the heart with DILP2 peptide (red) localized in the IPC processes (yellow in merge) and in punctate distribution on the heart, outside and graded in intensity away from the IPC processes. Scale, same as (B). (**D**) Side-on view of the heart shows the IPC processes [green, labeled as in (A)] and DILP2 peptide (red) are in contact with the heart epithelium (blue, labeled by antibody to myosin heavy chain) outside the heart lumen (asterisk) and facing the hemolymph. Scale bar, 10 μm. (**E**) A subset of corpora cardiaca cells that accumulate DILP2 peptide (green) specifically express AKH mRNA (red). Scale bar, 50 μm. White arrow, IPC cell bodies; pink arrow, heart-associated IPC processes. Black and white single images are shown (right) to clarify signal overlap. (**F**) A summary depiction of brain IPC anatomy and associated structures including observations not shown as data but described in the text. Green solid line indicates an IPC cell cluster from one side and its processes; green dashed lines indicate release sites of IPCs where DILP2 is seen outside the cells of synthesis.

ceased. The IPC-ablated larvae had an average combined glucose and trehalose level of 38% above normal, and these levels returned to normal when DILP2 was provided systemically by the transgene (Fig. 1C). Elevated hemolymph carbohydrate levels in larvae lacking IPCs indicate that insulin is an essential regulator of energy metabolism in *Drosophila*. This accumulation of carbohydrate in the blood is reminiscent of that seen in human diabetes mellitus, although it should be noted that we measured carbohydrate levels during development rather than in adults.

To investigate how central nervous system (CNS)–derived insulin regulates systemic functions, we examined the *Drosophila* IPC contacts outside the CNS. The morphology of the brain IPCs was examined with the use of the *dilp2* promoter to drive expression of mGFP, a membrane bound green fluorescent protein (GFP) (Fig. 2, A to C). The IPC clusters within the pars intercerebralis extend processes that terminate at the lateral protocerebrum and subesophageal ganglion. IPC processes also terminate on the heart and in the corpora cardiaca (CC) compartment of the ring gland, after crossing the midline and exiting the CNS (Fig. 2F). Labeling of the IPC processes with mGFP and DILP2 antibody (fig. S1) revealed localization of DILP2 peptide within the processes that contact the heart and ring gland (Fig. 2A). DILP2 peptide was concentrated in a graded distribution outside the cells of synthesis on the heart (Fig. 2C), and colabeling with myosin heavy chain antibody, which labels the columnar heart epithelium, showed that the IPC processes and DILP2 were localized outside the lumen of the heart (Fig. 2D). These results suggest the heart surface may be the site of insulin release to the openly circulating hemolymph. We propose that brain IPCs are essential for organismwide growth control and carbohydrate homeostasis through release of insulin peptides into circulating hemolymph. These cellular functions are notably similar to those of mammalian pancreatic β cells (*6*, *7*).

In *Drosophila* (*8*) and other insects (*9*), a fraction of CC cells synthesize adipokinetic hormone (AKH). AKH resembles glucagon in its activation of glycogen phosphorylase through heteromeric GTP-binding protein (G protein) and adenosine 3′,5′-monophosphate (cAMP) signaling to elevate blood sugar (*10*), and the two proteins have some limited sequence similarity (fig. S5). Double labeling of AKH mRNA and DILP2 peptide showed that IPCs extend processes to the CC and that AKH-expressing cells contain DILP2 (Fig. 2E). We also found that CC cells accumulate DILP2 within membrane-bound particles of the perinuclear space, suggesting the possibility that DILP2 is taken up by AKH cells (fig. S6). We cannot formally rule out the possibility that *dilp2* is transiently or minutely transcribed by AKH cells, although we have not detected expression of either the *dilp2* promoter or *dilp1*, *-2*, *-3*, and *-5* mRNAs in the AKH cells. Thus, in addition to contacts between IPCs themselves, the primary sites of IPC contact outside the CNS are the heart and the CC. Though they lack strict morphological homology, these intercellular contacts are analogous to the association of pancreatic β cells with other β cells, with glucagon-expressing α cells, and with blood vessels in the islets of Langerhans (*7*) and may reflect underlying evolutionary conservation.

Thus, there is remarkable similarity of the organ systems underlying conserved insulin function in diptera and mammals. Moreover, the presence of IPCs in the nervous systems of other invertebrate and protochordate species (*1*, *11–14*) and in primary cell cultures from mammalian fetal brain (*15*) provides further evidence for a common ancestral insulin-producing organ of neural origin. Our results also raise the possibility that common mechanisms of cell specification regulate development of pancreatic β cells and *Drosophila* brain IPCs.

References and Notes

1. W. Brogiolo *et al.*, *Curr. Biol.* **11**, 213 (2001).
2. S. L. McNabb *et al.*, *Neuron* **19**, 813 (1997).
3. C. Chen, J. Jack, R. S. Garofalo, *Endocrinology* **137**, 846 (1996).
4. R. Bohni *et al.*, *Cell* **97**, 865 (1999).
5. G. R. Wyatt, *Annu. Rev. Entomol.* **6**, 75 (1961).
6. B. Duvillie *et al.*, *Proc. Natl. Acad. Sci. U.S.A.* **94**, 5137 (1997).
7. E. P. Joslin, C. R. Kahn, G. C. Weir, *Joslin's Diabetes Mellitus* (Lea & Febiger, Philadelphia, PA, ed. 13, 1994).
8. B. E. Noyes, F. N. Katz, M. H. Schaffer, *Mol. Cell. Endocrinol.* **109**, 133 (1995).
9. H. F. Nijhout, *Insect Hormones* (Princeton Univ. Press, Princeton, NJ, 1994).
10. S. F. Vroemen, D. J. Van der Horst, W. J. Van Marrewijk, *Mol. Cell. Endocrinol.* **141**, 7 (1998).
11. H. Kondo, M. Ino, A. Suzuki, H. Ishizaki, M. Iwami, *J. Mol. Biol.* **259**, 926 (1996).
12. A. B. Smit *et al.*, *Nature* **331**, 535 (1988).
13. S. B. Pierce *et al.*, *Genes Dev.* **15**, 672 (2001).
14. J. E. McRory, N. M. Sherwood, *DNA Cell Biol.* **16**, 939 (1997).
15. D. W. Clarke, L. Mudd, F. T. Boyd Jr., M. Fields, M. K. Raizada, *J. Neurochem.* **47**, 831 (1986).

16. We thank K. Willert for help in antibody production, J. Peterson for help with in situ hybridization, and M. Fish for help with P element transformation. Supported by the Juvenile Diabetes Research Foundation (E.J.R.) and the Pew Charitable Trusts (S.K.K.).

Supporting Online Material

(www.sciencemag.org/cgi/content/full/296/5570/1118/DC1)

Materials and Methods

figs. S1 to S6

22 January 2002; accepted 1 April 2002

Stability in Real Food Webs: Weak Links in Long Loops

Anje-Margriet Neutel,[1]* Johan A. P. Heesterbeek,[2] Peter C. de Ruiter[1]

Increasing evidence that the strengths of interactions among populations in biological communities form patterns that are crucial for system stability requires clarification of the precise form of these patterns, how they come about, and why they influence stability. We show that in real food webs, interaction strengths are organized in trophic loops in such a way that long loops contain relatively many weak links. We show and explain mathematically that this patterning enhances stability, because it reduces maximum "loop weight" and thus reduces the amount of intraspecific interaction needed for matrix stability. The patterns are brought about by biomass pyramids, a feature common to most ecosystems. Incorporation of biomass pyramids in 104 food-web descriptions reveals that the low weight of the long loops stabilizes complex food webs. Loop-weight analysis could be a useful tool for exploring the structure and organization of complex communities.

An increasing number of studies provide evidence for the occurrence in real biological communities of patterns of interaction strengths that are important to community stability (*1–8*). Such patterns are characterized, for example, by strong links embedded in a majority of weak links (*1*, *2*, *6*) or by strong links concentrated on the lower trophic levels (*5*). However, there remains a need to determine which food-web properties cause the patterns, and to understand the exact form of the patterns and how they influence stability. Here we analyze the stabilizing properties of observed patterns in food webs (*5*, *9*) by looking at the distribution of interaction strengths (*10*, *11*) over trophic loops (*12–14*) of different lengths.

We carried out our first analysis with

[1]Department of Environmental Sciences, Utrecht University, Post Office Box 80115, 3508 TC Utrecht, Netherlands. [2]Faculty of Veterinary Medicine, Quantitative Veterinary Epidemiology Group, Utrecht University, Post Office Box 80151, 3508 TD Utrecht, Netherlands.

*To whom correspondence should be addressed. E-mail: a.neutel@geog.uu.nl